metals

MDPI

Article

Bayesian Correlation Prediction Model between Hydrogen-Induced Cracking in Structural Members

Taejun Cho [1,†], David Joaquin Delgado-Hernandez [2], Kwan-Hyeong Lee [3], Byung-Jik Son [4] and Tae-Soo Kim [5,*]

1 Department of Civil Engineering, Daejin University, Hogookro 1007, Pocheon 11159, Korea; taejun@daejin.ac.kr
2 Postgraduate Engineering Department, Autonomous University of the State of Mexico, Toluca 50130, Mexico; delgadoh01@yahoo.com
3 Department of Robotics Engineering, Daejin University, Hogookro 1007, Pocheon 11159, Korea; khlee@daejin.ac.kr
4 Department of International Civil and Plant Engineering, Konyang University, Nonsan 35365, Korea; strustar@konyang.ac.kr
5 Department of Architectural Engineering, Hanbat National University, Daejeon 34158, Korea
* Correspondence: tskim0709@daum.net; Tel.: +82-42-821-1121
† Current address: Sinwondang 103–708, Sungsa, Goyang, Geyeongi 10455, Korea.

Academic Editors: Ricardo Branco and Filippo Berto
Received: 19 March 2017; Accepted: 31 May 2017; Published: 5 June 2017

Abstract: Background: A quantitative model was developed and applied for analyzing the correlation between hydrogen-induced corrosion cracking in both main cable wires and degraded stiffening of the girders of a cable suspension bridge, considering maintenance effects across time and space. Method: Bayesian inference is applied for predicting the correlations among the wires in the main cables owed to hydrogen-induced cracking (HIC) in the cable wires of a steel bridge, by using the improved hierarchical Bayesian models proposed here. Results: The simulated risk prediction under decreased strength of cable wires, due to the corrosion cracking, yields posterior distributions based on prior distributions and likelihoods. The Bayesian inference model can be applied to the design and maintenance of highly corroded and correlated components Data are updated through analyzed information from previous crack steps. A numerical example including not only reliability indices but also probabilities of failure for cable wires, damaged by HIC, is then presented. Compared with a conventional linear prediction model, the one herein developed provides highly improved convergence and closeness to the analyzed data. Conclusion: The proposed model can be used as a diagnostic or prognostic prediction tool for the performance of corroded bridge cable wires with crack propagation, allowing the development of maintenance plans for mechanical components and the overall structural system.

Keywords: corrosion; cable wires; hydrogen-induced cracking; hierarchical Bayesian inference; correlation model; maintenance interventions

1. Introduction

As a mixture of corrosion and crack growth deterioration in structural steel, Hydrogen-Induced Cracking (HIC) has been present in the cable wires of many suspension bridges [1–9]. Because it may become the primary cause underlying abrupt failure of structural systems, HIC of cable wires is a critical issue in cable-supported structures. However, very few studies have attempted to quantify the correlation between HIC and structural components. The quantification of this correlation is essential for developing an optimized maintenance plan in terms of budget management, leading to the design

of appropriate rehabilitation methods, to the location of damaged members, and to the identification of maintenance tasks. Therefore, this piece of research introduces HIC and a method for quantifying the deterioration of steel members in structural systems.

Corrosion reactions often result in the formation of hydrogen gas. Hydrogen atoms can either diffuse or be absorbed into the lattice of the metal, leading to the deterioration of material properties. This, combined with the stress applied to the metal, can result in crack propagation. Diffused hydrogen atoms can recombine to form hydrogen molecules, which can exert pressure on the surrounding steel, resulting in the crack propagation in wires under high tensile stress [3,4].

Such corrosion can happen under exposure to carbonated and bicarbonated, caustic, nitrate, cyanide, anhydrous ammonia (liquid), mixture of nitric and sulfuric acid, mixture of magnesium chloride and sodium fluoride, or $CO/CO_2/H_2O$ mixtures, and under hydrogen attack. Some mechanisms have been proposed in the literature for explaining the phenomenon; these can be classified as either anodic Stress Corrosion Cracking (SCC) mechanisms or mechanical fracture processes. Anodic SCC involves the rupture of the protective oxide layer at the crack tip, anodic dissolution of the base metal, and crack growth under constant stress. Crack growth in turn can be intergranular or transgranular [10].

Another similar concept is that a film is formed on a metal surface, and brittle fracture follows due to dealloying or vacancy injection. The crack proceeds through the film and across the film/metal interface into the metal, where it propagates under the stress of the applied load. Once the crack propagation stops, the process restarts with the formation of a new film. It is worth noting that this mechanism is a combination of Hydrogen-Assisted Cracking (HAC) and SCC [11].

The differences between SCC and HAC have been investigated by Wen-Ta Tsai et al. [11]. Depending on the potential, the types of and reasons underlying, SCC vs. HAC are different. In their tests, when the potential was moved towards the cathodic direction (<-900 mVSCE; millivolts silver chloride and saturated calomel), HAC was observed. The loss of ductility, as indicated by a decrease in the reduction in the area of the specimen, as compared to that in an air test, was linked to crack initiation and propagation. In short, hydrogen plays a key role in many cracking mechanisms including SCC and HAC. HAC encompasses a number of different mechanisms and, in some cases, is considered to be interchangeable with HIC, hydrogen embrittlement and hydrogen damage.

The mechanism of HIC begins with the hydrogen atoms diffusing throughout the material. At elevated temperatures, hydrogen tends to have increased solubility, allowing it to disperse into the material. When such hydrogen atoms combine again in very small metal voids to build molecules of hydrogen, they produce pressure within the cavity. The pressure created from the buildup can further elevate, which makes the metal to lose its tensile strength and ductility, reaching the cracking point, or HIC [12].

Hydrogen-Induced Cracking (HIC) refers to the internal cracks brought about by the material trapped in budding hydrogen atoms. It involves atomic hydrogen, which is the smallest atom, diffusing into a metallic structure. In the case of a crystal lattice becoming saturated or coming into contact with atomic hydrogen, many alloys and metals may lose their mechanical properties.

If the buildup of molecular H is repressed, the emerging atomic H can disperse into the metal rather than forming a gaseous reaction. This, in turn, produces a crack in the metal. Certain chemical elements may contribute to this phenomenon, such as selenium, antimony, arsenic and cyanides. However, the main one is H_2S, or hydrogen sulfide.

In this study, the focus is on the reduction of ductility and tensile strength due to the hydrogen absorption in high-strength steel, which ultimately results in the brittle failure of a structural system. Moreover, the research allowed the authors to develop a correlation model for predicting the HIC in cable wires and steel members of target structural systems.

Although there are strong correlations among sources of corrosion and cracking in steel wires and other members in steel structures, a quantitative correlation model for modeling them has scarcely been investigated. In terms of the HIC of the cables of a suspension bridge, the local and global safety

of bridge systems have been compared by the authors of this study and by other researchers [3,4,11,13]. With regard to the local safety analysis, a decoupling technique based on two-dimensional finite element models has been developed for evaluating hydrogen-diffusion-driven crack propagation in a wire section. A serviceability limit state based on the global responses of a stiffening girder, the ultimate limit state, and the reliability of time-dependent and crack depth-dependent HIC of a cable wire has been calculated for individual components. Parallel system reliability analyses have also been carried out. While the proposed solutions show local and global risks successfully and separately calculated based on observed differences in the global and local safety behaviors of the suspension bridge system, a quantitative correlation between the two behaviors has not been modeled [3,4].

The correlation quantification among risky elements is important, especially when the components of a complex system are highly correlated. Predicting future degradation through the application of stochastic regression models needs additional consideration given their synergistic or dependent causes, which may result in growing damages. Thus far, efforts to determine correlations among the causes of deterioration and results have focused on only a few variables. For example, HIC in the main cables of a suspension bridge could beget torsion stress in stiffening girders [14] or nuts being pulled off in hangers. Hence, it is necessary to identify the correlations among the causes of deterioration and their results for an appropriate bridge management system, followed by the prediction of crack propagation in cable wires due to HIC.

For analyzing these correlations and the resulting deterioration, conventional stochastic modeling of structural components and systems has been applied mainly on the basis of Event Tree Analysis (ETA) [15], Fault Tree Analysis (FTA) [16], and regression simulation in terms of the Response Surface Method (RSM) or adaptive RSM [17,18]. ETA is a method for illustrating the sequence of outcomes that may arise after the occurrence of a selected initial failure event and for ranking accidents, considering that the order of events needs permutation-based calculations, which produce a large number of cases for predicting failure scenarios.

Modeling uncertainties in environmental load components could be considered in a correlation analysis by conducting uncertainty analysis between the resultant stress ranges and the expected fracture lives, due to hydrogen-induced corrosion cracking based on Bayesian inference modeling. Compared with ETA or FTA, the Bayesian inference model could evaluate and detect the partial failure as a probabilistic quantification, which is allowed neither in ETA nor in FTA.

Bayesian analysis is based on posterior inference [19]. Parameter estimates are usually summary statistics of the marginal posterior distributions such as the posterior mean, median, mode, and standard deviation. In nonhierarchical Bayesian models, it is often easy to analytically derive the marginal posterior distributions and obtain the summary statistics. However, in highly correlated system models, specifically, given that the parameters are of multiple dimensions, it is often difficult to present the marginal distribution of each parameter analytically.

The results of this study could appreciably reduce the known limitations for predicting future degradation and enable the full modeling of field variables, which are highly correlated and show inelastic behavior. The limitations are as follows:

1. Most mechanical components affect future events because of the evaluation of joint probability distributions of current maintenance data, which are highly correlated among the components.
2. Modeling uncertainty, when multiple parameters can be regarded as related or connected in some manners due to hydrogen-induced corrosion cracking, implies that a joint probability model should reflect the dependence among these parameters, which could then be modeled in a hierarchical inference.
3. Prediction of future degradation of a component or a structural system is performed through the implementation of an updated stochastic model; reducing errors arising from corroded and correlated components, nonlinear behaviors, and including maintenance interventions as well.

With these ideas in mind, the objectives and scope of this paper are:

- To assess risk correlation between shear and bending deformation of steel members and HIC in high-strength steel of main cable wires.
- To simulate degradation of cable wires on the basis of the proposed Bayesian prediction models in terms of locally correlated cracking in cable wires just before the collapse of a structural system, considering maintenance interventions by implementing an inverse analysis of the proposed Bayesian inference network model.

2. Bayesian Hierarchical Model for Correlated Data

2.1. Hierarchical Modeling

Bayes' theorem gives the posterior distribution for the parameters of interest, in terms of the prior distribution, failure model, and the observed data, which in the general continuous form is written as [14]:

$$\pi_1(\theta|x) = \frac{f(x|\theta)\pi(\theta)}{\int f(x|\theta)\pi(\theta)\mathrm{d}\theta}, \quad (1)$$

where, $\pi_1(\theta \mid x)$ is the posterior distribution for the parameter of interest, denoted as θ. The observed data enter via the likelihood function, $f(x \mid \theta)$, and $\pi(\theta)$ is the prior distribution of θ. $f(x)$ is called the marginal or unconditional distribution of x. The range of integration is over all possible values of θ, being the probability of seeing x events, referred to as the predictive distribution for x [15].

Hierarchical models have been introduced in population-based problems [16], describing efficiently complex datasets incorporating correlation. Hence, when multivariate or repeated responses are observed, correlation can be included in the model via random effect for all measurements referring to the same individual. Random effects and the corresponding hierarchical structure are applied to appropriately specify the marginal sampling distribution frequently referred to as data augmentation, which has been considerably simplified in the Markov Chain Monte Carlo methods (MCMC) scheme that can be used to estimate the posterior distributions of interest. One of the MCMCs, Metropolis Hastings (M-H) sampling [17] numerically and efficiently simulates posterior distribution of parameters, which has been adopted in this study.

2.2. Hierarchical Bayesian Inference Model to Predict Degradation of Cable Wires due to HIC

In order to reconstruct incompletely observed or missing data, imputation models are commonly selected, which include the regression method for monotone data, the non-parametric Propensity method [18], and the MCMC [16] for non-monotone cases. In this research, creating a predictive distribution has been applied based on predictive distributions, while the data are averaged over all possible parameter values for the maintenance data of a bridge structure. The validation of the suggested model has been compared with the measured maintenance data with the partially deleted input prior distribution data.

For this reason, when datum y has not been observed yet, predictions are based on the marginal likelihood:

$$f(y) = \int f(y|\theta)f(\theta)\mathrm{d}\theta, \quad (2)$$

which is the likelihood averaged over all parameter values supported by prior beliefs, where, $f(y)$ is called prior predictive distribution.

The posterior predictive distribution is given by:

$$f(y'|y) = \int f(y'|\theta)f(\theta|y)\mathrm{d}\theta, \quad (3)$$

which is the likelihood of the future data averaged over the posterior distribution $f(\theta|y)$.

This distribution is termed as the predictive distribution since prediction is usually attempted only after observation of a set of data y. Future observations y' can be alternatively viewed as additional parameters under estimation. From this perspective, the joint posterior distribution is now given by $f(y', \theta|y)$. The MCMC method is used to obtain this posterior distribution from which the imputed values for missing observations or future predicted data are drawn. Inference on the future observations y' can be based on the marginal posterior distribution $f(y'|y)$ by integrating out all nuisance parameters, one of which in this case, is the parameter vector θ. Hence, the predictive distribution is given by Equation (3), since past and future observables, y and y', are conditionally independent given the parameter vector θ [19].

Linear regression models are common in statistical sciences. In linear regression models, the response variable Y is considered to be a continuous random normally distributed variable defined in the whole set of real numbers. The following equation is selected:

$$Y_{ij} = \alpha_i + \beta_i(x_j - \overline{x}), \tag{4}$$

where $\overline{x}$ = mean value of maintenance (duration of service). Due to the absence of a parameter representing the correlation between α_i and β_i, standardizing the x_j's around their mean to reduce dependence between α_i and β_i in their likelihood is carried out, achieving complete independence.

The synergic effects have been evaluated in deterministic and probabilistic ways, which revealed worse deterioration than linearly superposed. Therefore, the following quadratic regression models are proposed, for which each dependent variable serves as the dependent variable and the other variables in the dataset serve as the independent variables:

$$Y_{ij} = \alpha_i + \beta_i(x_j - \overline{x}) + \gamma_i(x_j - \overline{x})^2, \tag{5}$$

The model parameter estimates are then used in making random draws from the multinomial distribution for each missing response on the dependent variable in the regression.

3. Correlation Model for HIC in the Main Cable Wires

3.1. Deterministic Global Analysis Model for HIC of High-Strength Steel Wires in Suspension Bridges

HIC propagation in cable wires of a suspension bridge has been analyzed previously [3,4]. The structural model of a cable suspension bridge has 336 frame elements, 242 catenary cable elements, and 461 node numbers (2766 degrees of freedom, Figure 1). The maximum response of a bridge system has been obtained for tensile stresses at two girder section locations in the center span (Figure 2). The maximum values of the shear stress and horizontal deformation are obtained when the live load is loaded at the side span.

There are two load cases for generating the maximum tensile and shear stresses. Case 1 is for generating the maximum tensile stress, which is the combination of dead load (DL), traffic or live load (LL), wind load (WL), and temperature load (TL). Case 2 is for generating the maximum shear stress, which is the combination of DL, WL, and TL, i.e., (DL + WL + TL). The stresses and deflections pertaining to Load Case 1 are evaluated at $L/4$ and $L/2$ of the central span (L refers to the length of the central span), i.e., elements 48 and 72, and nodes 199 and 223 (Figure 2). The stresses and deflections pertaining to Load Case 2 are evaluated at the end of the central span, i.e., element 2, and node 153 (Figure 2).

Experiments on hydrogen-induced corrosion cracking in cable wires of suspension bridges were conducted [20]. The prestressing tendon were tested by Toribio [21]. The experimental results were compared with the solutions yielded by the analytical equations of Forman and Shivakumar [22] and the author's FEM analysis program written for the ANSYS61 platform [3,4]. The test results of the experiments on the hydrogen-induced corrosion cracking of cable wires [20] and the reduced brittle failure strength of wires closely follow the constitutive relationship for undamaged new wires. Figure 3

shows that the cracks lead to sudden brittle failure for that crack depth for which the stress intensity factor at the crack tips was equal to the critical Stress Intensity Factor (SIF) or fracture toughness (K_c) of the material, which was determined using the aforementioned FE program [3], compared with Forman's theoretical equation for SIF [23].

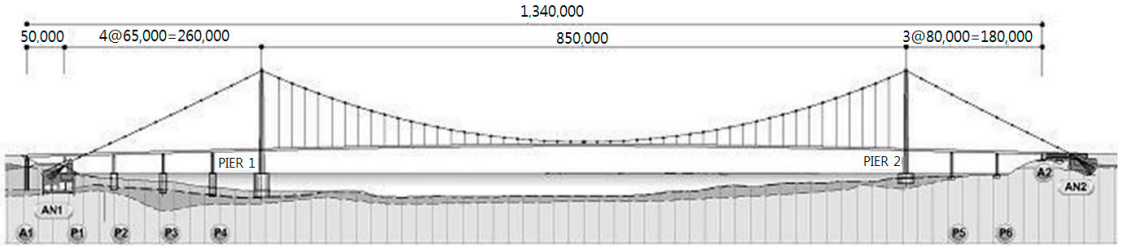


Figure 1. Side view of example suspension bridge (Unit: mm).

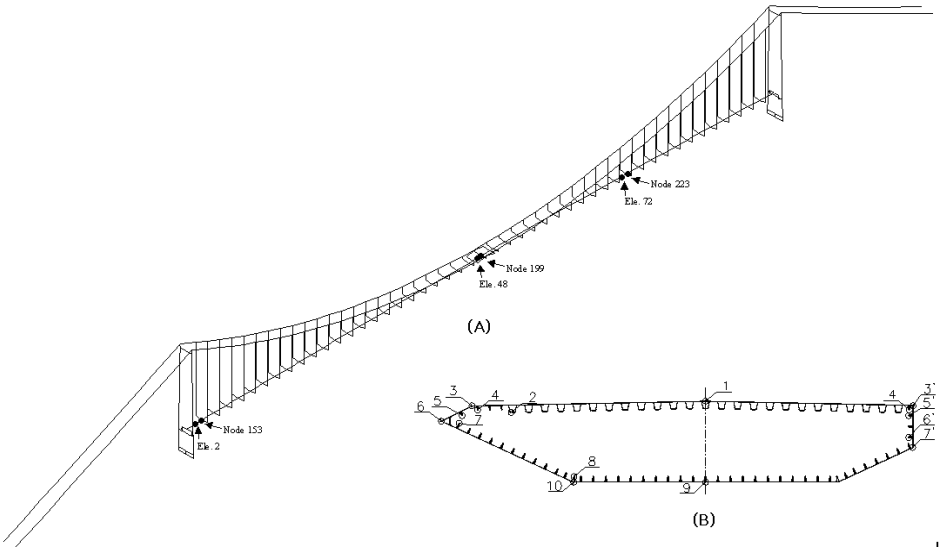


Figure 2. Observation positions of structural responses: (**A**) nodes and elements; and (**B**) cross section.

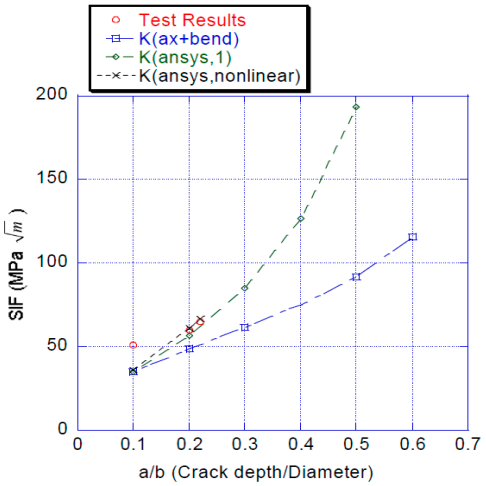


Figure 3. Constitutive relationship while the crack is growing in the main cables and the Calculated SIF is compared with the test results. Calculated SIF by elastic and elastic-plastic material behavior, compared with test results [3].

HIC of the main cable wires is directly related with the collapse of a suspension bridge. The safety and correlation of components with regard to the structural system has been determined using a decoupled FE analysis model and by conducting reliability analysis (Figure 4) in which only the local correlation of HIC in cable wires was measured.

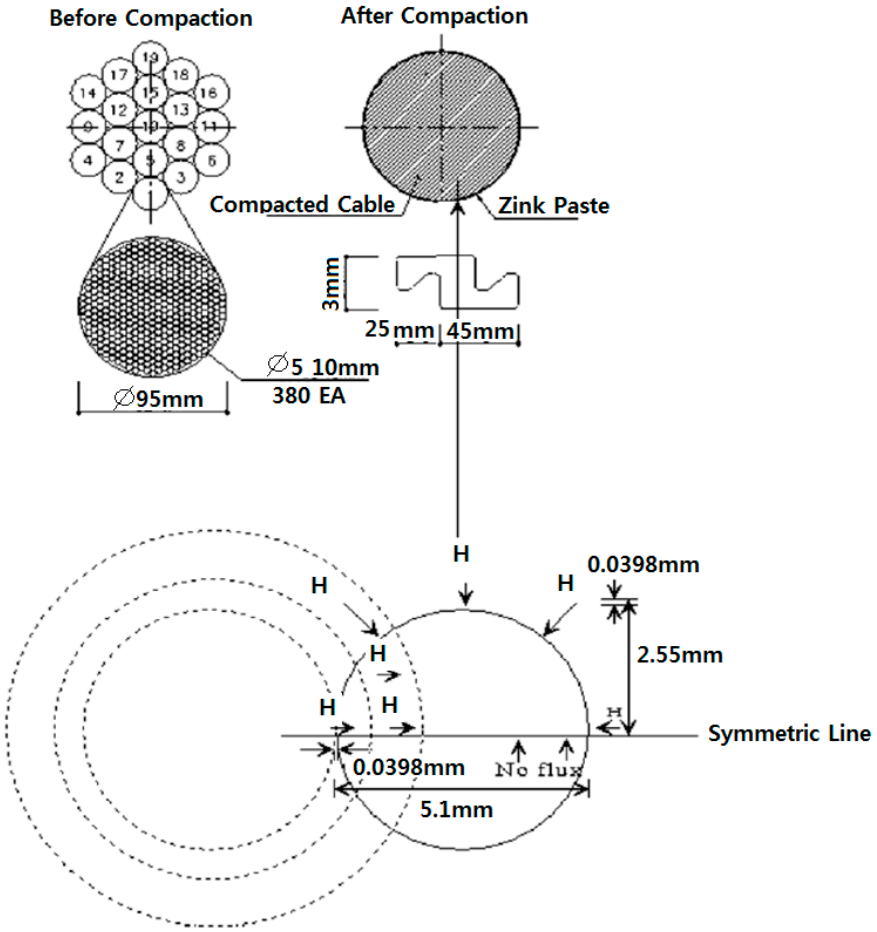


Figure 4. Finite Element Analysis model for crack propagation in main cable wires [3].

Considering periodical maintenance tasks, it would be helpful if the correlation between local and global components in terms of the HIC of cable wires and the structural responses of the bridge itself was quantified, which is described in the following section.

3.2. Correlation between Local and Global Component Reliabilities

Figure 1 presents the suspension bridge subjected to the evaluation of HIC and the overall dimension of the above stated bridge system. All stresses in the cross section are evaluated at the two positions, i.e., 1 and 2, as shown in Figure 2. The limit state functions for evaluating reliability indices and failure probabilities are composed of 10 cases, whereas the extent of corrosion of the main cable wires varies from 0 to 100%.

STEPs 1–6 mean 10–60% of the loss in the total 7220 wires, respectively. Hence, at Step 1, 722 wires are broken by HIC, and in Step 2, 1444 wires are fractured. For Step 6 in Figure 5, 4332 wires are removed from the active wires. While wires are broken, because the total loads are constant, the remaining wires will be more loaded. As tensile loads and stresses are increased in the wires, the diffusion of hydrogen atoms and the propagation rates of cracks into wires are accelerated. Consequently, the wires' lifetime is reduced. When the degree of corrosion is 60% in Step 6, the wires will reach the fracture toughness, K_c (45 MPa $\sqrt{m}$), immediately.

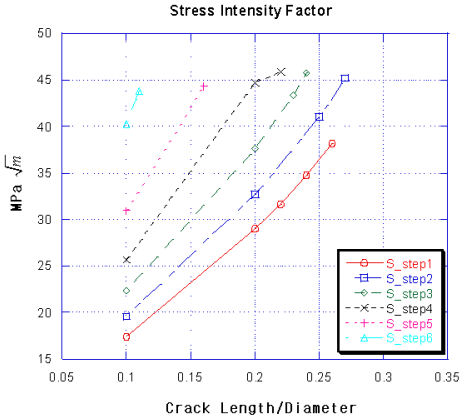


Figure 5. Stress Intensity Factor (K) while crack propagates in each degree of corrosion [3].

The reliability results for tensile and shear stresses are shown in Figures 6 and 7, respectively. As can be seen, for normally distributed random variables, the reliability index is related to the probability of failure by:

$$\beta = -\Phi(P_f) \text{ or } P_f = \Phi(-\beta), \quad (6)$$

where Φ^{-1} is the inverse standard normal distribution function, when P_f is less than 0, the probability of failure is larger than 50%. Table 1 compares several calculated reliability indices with the Probability of Safe, P_S, and the Probability of Failure, P_f.

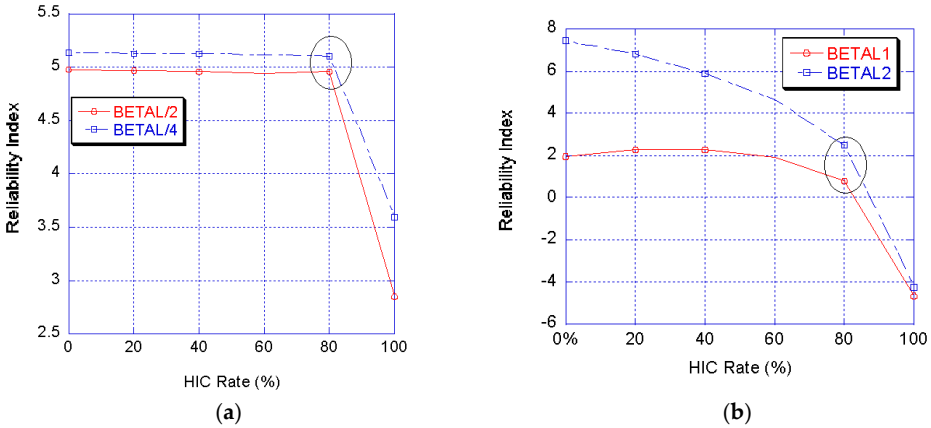


Figure 6. Reliability indices for tensile stresses and shear stresses in cable wires, where $L/4$ means span/4 (Node 223) and $L/2$ means span/2 (Node 199) (see Figure 2): (**a**) tensile stresses; and (**b**) shear stresses.

Table 1. Five Correlated cubic functional values with random effects.

X (Year)	Y_1	Y_2	Y_3	Y_4	Y_5
1	2.5	3.162463	2.393176	5.211623	3.625013
2	4	5.270988	3.154476	6.554857	6.958659
3	−0.5	−0.59202	−0.43391	−0.56402	−0.86762
4	−17	−24.256	−12.6095	−23.2487	−26.4017
5	−51.5	−68.6477	−42.3458	−89.3462	−96.6057
6	−110	−160.169	−87.4144	−184.485	−162.822
7	−199	−208.906	−141.385	−286.652	−269.2
8	−323	−359.445	−269.061	−364.23	−529.286
9	−490	−522.926	−374.941	−822.392	−604.255
10	−704	−716.606	−507.154	−989.295	−989.443

The following serviceability limit states are selected for the system reliability of a cable wire in two load cases and at two check points as a corrosion dependent function:

$$g(C) = \sigma_{cr} \times N_{\sigma_{cr}} - \left(a_0 + \sum_{i=1}^{n} a_i x_i + \sum_{i=1}^{n} a_i x_i^2 \right), \quad (7)$$

$$g(C) = \tau_{cr} \times N_{\tau_{cr}} - \left(a_0 + \sum_{i=1}^{n} a_i x_i + \sum_{i=1}^{n} a_i x_i^2 \right), \quad (8)$$

where σ_{cr} is the code specified allowable tensile stress (190 MPa), as a resistance value; τ_{cr} is the code specified allowable shear stress (110 MPa); and $N_{\sigma_{cr}}$ and $N_{\tau_{cr}}$ are the bias factors of tensile stress and shear stress respectively. The values in parenthesis are the corrosion dependent tensile and shear stresses, responses of the bridge system when the areas of the main cables and hangers are perturbed, as a load term.

The selected random variables are about three kinds of cable section area. Since the Bucher-Bourgund method [24] is employed, the three axial points have the distances of $\pm\sigma$ (standard deviation) between the center and axis points. The time-dependent safety of each response is evaluated by applying Equations (6) and (9) for the component and system reliability, respectively.

The upper and lower bounds of the probabilities of failure in the positively correlated parallel system occur as follows [17].

$$\prod_{i=1}^{n} F_{Ri(q)}(t) = \prod_{i=1}^{n} P_{fi}(t) \leq \Phi\left(-\beta_e \times \sqrt{\frac{n}{1+(n-1)\bar{\rho}}} \right) \leq P_f(t) \leq \min(P_{fi}(t)), \quad (9)$$

where P_f is the probability of failure of the parallel-connected structural system; $F_{Ri(q)}(t)$ is the cumulative distribution function; q_i is the normalized base variables of load; and P_{fi} is the probability of failure of the ith component, which is calculated by standard normal distribution as $P_{fi} = \Phi(-\beta_i)$; n is the number of parallel elements, and $\bar{\rho}$ is the coefficient of partial correlations.

Figures 6 and 7 show that reliabilities decrease and the probabilities of failure increase when the HIC ratio is greater than 80%, as indicated with the black circles. If the degree of corrosion for wires due to HIC is greater than 60% (Figure 5, Fracture analysis result), the cable wires will fail immediately. Note that all wires are fully correlated via the hierarchical Bayesian prediction model.

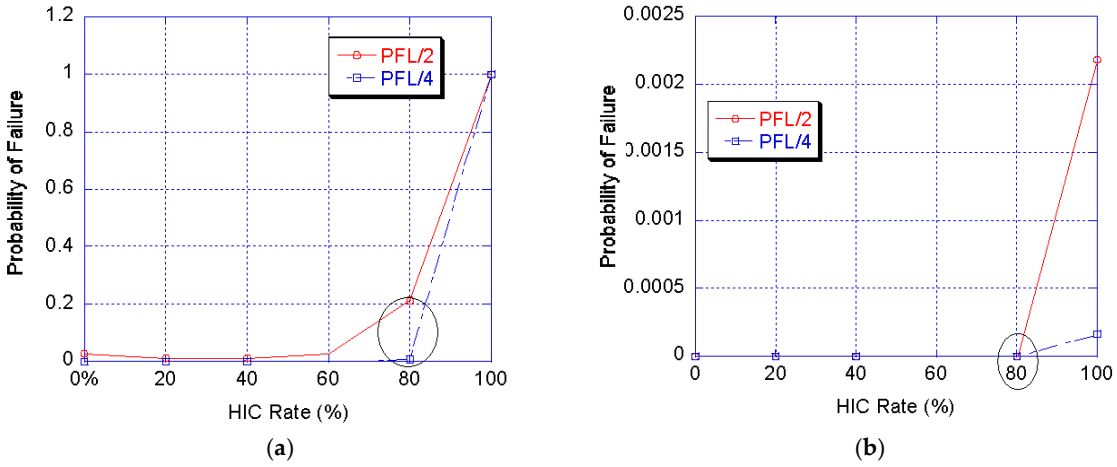


Figure 7. Failure probabilities for tensile stresses and shear stresses in cable wires, where $L/4$ means span/4 (Node 223) and $L/2$ means span/2 (Node 199) (see Figure 2): (**a**) tensile stresses; and (**b**) shear stresses.

As shown in Figure 8, although the expected mean values have slightly higher indices (less risky) than the calculated reliability indices, the confidence intervals or the predicted distributions of the predicted values incorporate the previous calculations shown in Figure 9 for the tensile and shear stresses' reliability indices.

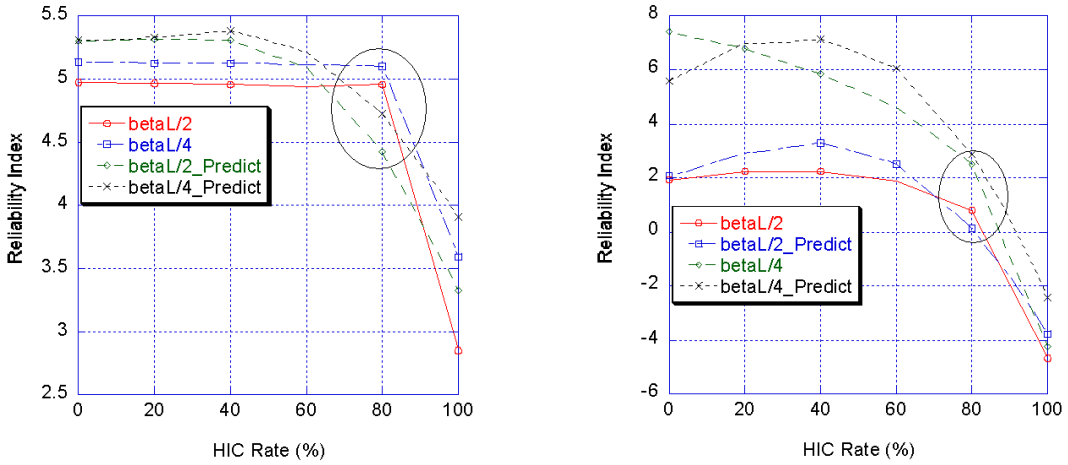


Figure 8. Predicted reliability indices for tensile and shear stresses in cable wires, where $L/4$ means span/4 (Node 223) and $L/2$ means span/2 (Node 199) (see Figure 2): (**a**) tensile stresses; and (**b**) shear stresses.

The correlation model between tensile stress and shear stress could be very important for identifying the correlation between the shear and tensile stress responses, in which data measured during daily monitoring show correlated responses from correlated structural behaviors in the target structure. In addition, shear stresses show sharper responses than other types of stresses, as shown in Figures 8 and 9. The correlation modeling and the resulting Bayesian belief network are discussed in the following section.

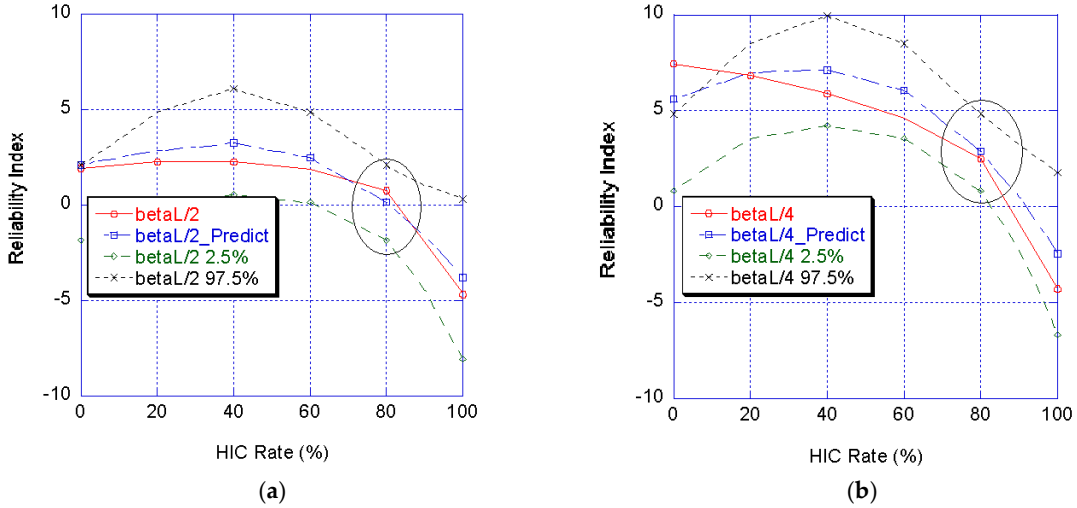


Figure 9. Confidence intervals of predicted reliability indices for shear stresses in cable wires, where $L/4$ means span/4 (Node 223) and $L/2$ means span/2 (Node 199) (see Figure 2): (**a**) tensile stresses; and (**b**) shear stresses.

3.3. Dynamically Correlated System Responses due to the Main Cable Crack Growing

While crack propagated in strands of main cable from 0 to 100%, tensile and shear stresses in stiffening girders increase. The proposed quadratic Bayesian prediction model is applied while strands have failed in terms of local modeling of HIC in wires of strands. After the local prediction modeling, correlation model could be applied to identify the correlation between shear and tensile stress responses, which can be important criteria of maintenance before determining appropriate management tasks.

The probability density function based on the joint probability, following the Markov condition is calculated as:

$$P(X_{1:T}) = \prod_{t=1}^{T}\prod_{i=1}^{n} P(X_t^i \Big| \pi(X_t^i)), \tag{10}$$

where X_i represent nodes, and parents represent the stress responses at stiffening girders. T is the crack propagation time in unit of percentile from 0 to 100%.

The time dependent coefficients of correlation among nodes are:

$$\rho_{xy}^t = \frac{1}{n} \frac{\sum_{t=1}^{T}\sum_{i=1}^{n} x_i^t y_i^t - \sum_{t=1}^{T} \overline{xy}}{\sum_{t=1}^{T} S_x^t S_y^t}, \tag{11}$$

where ρ_{xy}^t is the correlation coefficient between random variables, x_i^t and y_i^t denote the random variables, n represents the total number of random variables, S_x^t and S_y^t are the standard deviations of the variables, and $\overline{x}, \overline{y}$ are the mean values of the random variables at time t.

A Dynamic Bayesian Belief Network model (DBBN) was employed here, as shown in Figure 10. After 100,000 iterations of the Markov Chain Monte Carlo simulation, the following correlations between tensile and shear stresses in stiffening girders were observed in Figure 11. In the figure, correlations between tensile and shear stresses at $L/2$ and shear stress at $L/4$ are plotted while crack propagates from 0 to 100%.

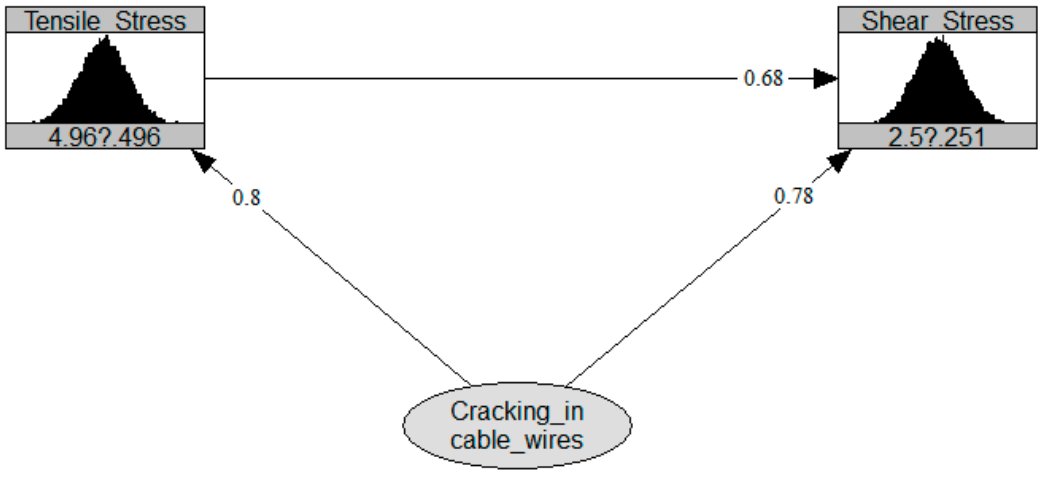


Figure 10. Random variables modeled with nodes and arcs using Uninet version 2.74 (LightTwist Software, Melbourne, Australia).

As shown in Figure 11, there are higher correlations between the tensile stresses at $L/2$ and $L/4$, which are the same for shear stresses at two girder locations because the value is on average higher than 0.3 between mu[1,*] and [2,*], where * means crack propagation steps. The percentile, mean, standard deviation, and error of MCMC is presented within the Appendix A in Table A1. The quantity

reported in the MC error column gives an estimate of σ/N1/2, the Monte Carlo standard error of the mean.

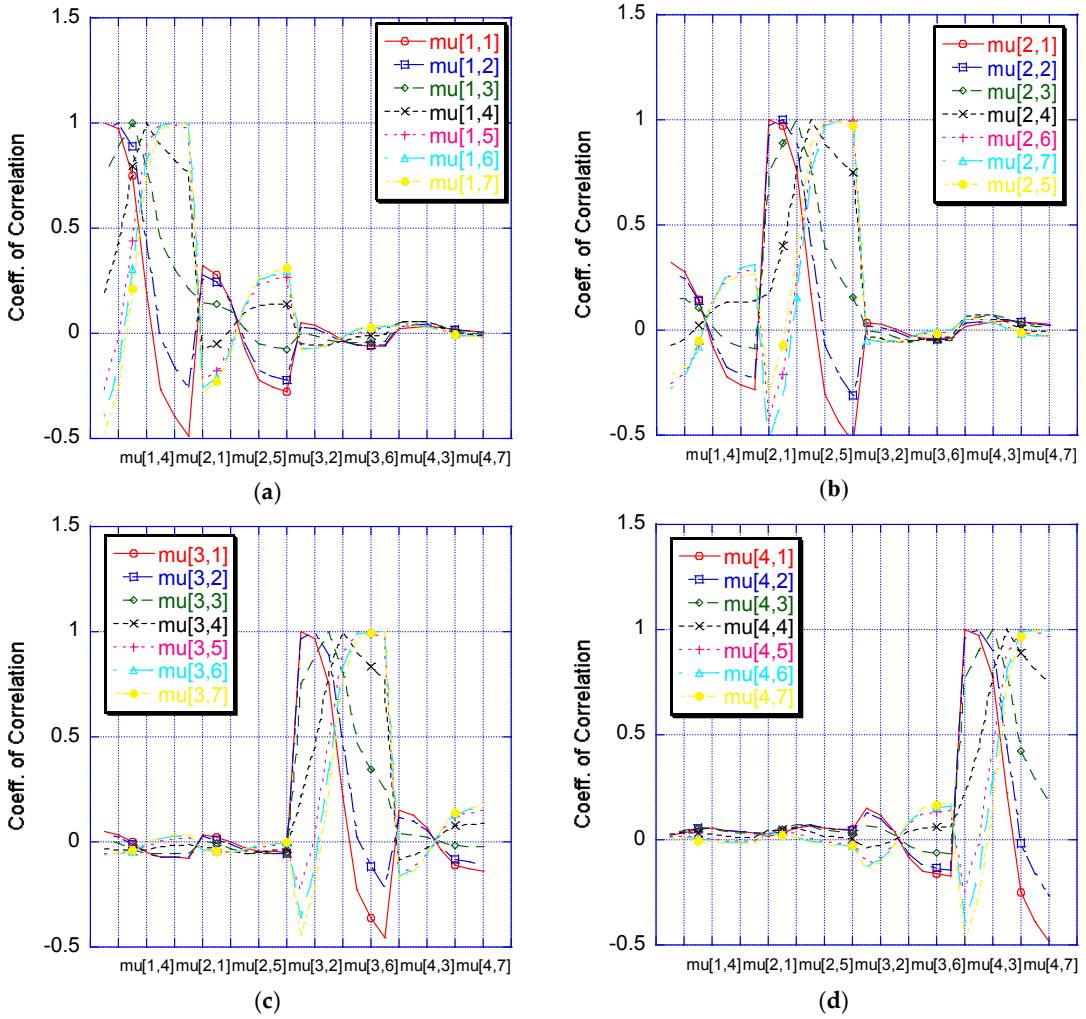


Figure 11. Correlations between tensile and shear stresses at $L/2$ and shear stress at $L/4$, where $L/4$ means span/4 (Node 223) and $L/2$ means span/2 (Node 199) (see Figure 7). Here, for mu[x, y], x = 1,2 implies tensile stress at $L/2$ and $L/4$; x = 3, 4 implies shear stress at $L/2$ and $L/4$; and y = 1 to 7 implies crack propagation from 0 to 20%, 40%, 60%, 80%, 90%, and 100%, respectively. (**a**) Tensile stress at $L/2$ and other variables. (**b**) Tensile stress at $L/4$ and other variables. (**c**) Shear stress at $L/2$ and other variables. (**d**) Shear stress at $L/4$ and other variables.

This value increases as the crack propagates through the main cable wires. The difference in the level of correlation at the two aforementioned locations indirectly proves that given the difference in these responses, there is little effect of the imposed direct load on the girder. This inference contradicts Betti-Maxwell's reciprocal theorem, but proves that they are dependent on the HIC in the main cable wires.

On the basis of these observations, the reference response to shear stresses at $L/4$ could be important in determining the risk stages for the considered structural system. However, two major problems can arise in the case of maintenance interventions for replacing the main cable wires or reinforcing the girder; for instance, increasing the sectional area or moment of inertia would lead to a change in the tensile or shear responses.

In those cases, a modified response should be determined for identifying the source of deformation, i.e., crack propagation in the main cable wires, which can be calculated based on the proposed inverse

DBBN model and Equation (11). Two cases of stiffening girder are considered, which is reinforced by widening or thickening the girder's flanges. Hence, the two reinforced girder cases are modeled as decreasing tensile stresses from 100% to 25% and 50% under 80% crack propagation in the wire, as summarized in Table 2.

Table 2. Reliability Index versus Probability of Failure.

Reliability Index	Reliability, P_S (=1 − P_f)	Probability of Failure, P_f
0	0.5	0.5
0.5	0.691	0.309
1	0.841	0.159
1.5	0.9332	6.68×10^{-2}
2	0.9772	2.28×10^{-2}
2.5	0.99379	6.21×10^{-3}
3	0.99865	1.35×10^{-3}
3.5	0.999767	2.33×10^{-4}
4	0.9999683	3.17×10^{-5}
4.5	0.9999966	3.40×10^{-6}
5	0.999999713	2.87×10^{-7}
5.5	0.999999981	1.90×10^{-8}
6	0.999999999	9.87×10^{-10}
7	1	1.28×10^{-12}
8	1	6.11×10^{-16}

It would be important to vary the responses while changing the extent of crack propagation in the main cable wires from the viewpoint of maintenance tasks, involving replacing the main cable wires. Therefore, two cases of the main cable wire rehabilitation are considered. The reliability indices of the reinforced cable wires are assumed to increase from 0.5 to 3.0 and 5.0 under 80% crack propagation in the wires, as referenced from the replacement of cable wires in real structures [25]

The inverse Bayesian belief models are shown in Figure 12, in which the increased reliability indices of 3.0 and 5.0 are shown. All types of probabilistic distributions of the reliability indices of stresses and cracking in wires are assumed as normally distributed with a standard deviation of 0.1.

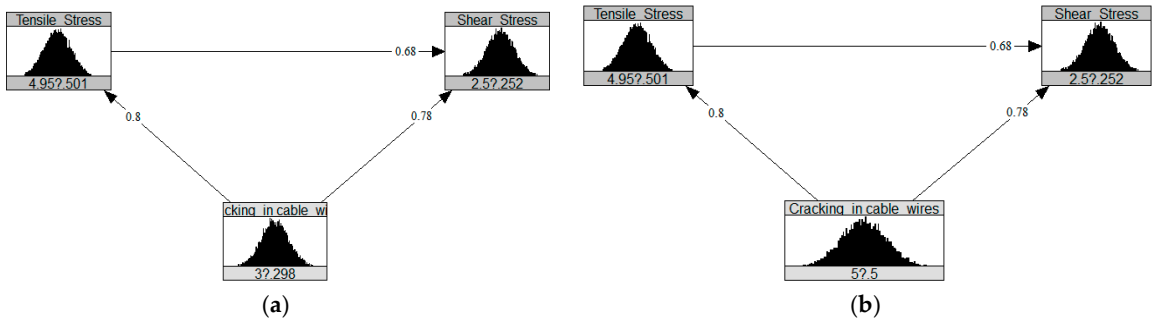


Figure 12. Inverse analysis of Bayesian belief network under 80% crack propagation in wire and reinforced as reliability indices increased from 0.5 to: (**a**) 3.0; and (**b**) 5.0. (**a**) Reliability index = 3.0 in cable. (**b**) Reliability index = 5.0 in cable.

Figure 13 shows the results of the inverse Bayesian belief network simulations in terms of the reliability indices for tensile and shear stress responses, while cracking in wire in 80% reinforced as the reliability indices increased from 0.5 to 3.0 and 5.0. Compared with the originally predicted indices, the reinforced main cable wires, having indices of 3.0 and 5.0, show reduced tensile and shear stresses.

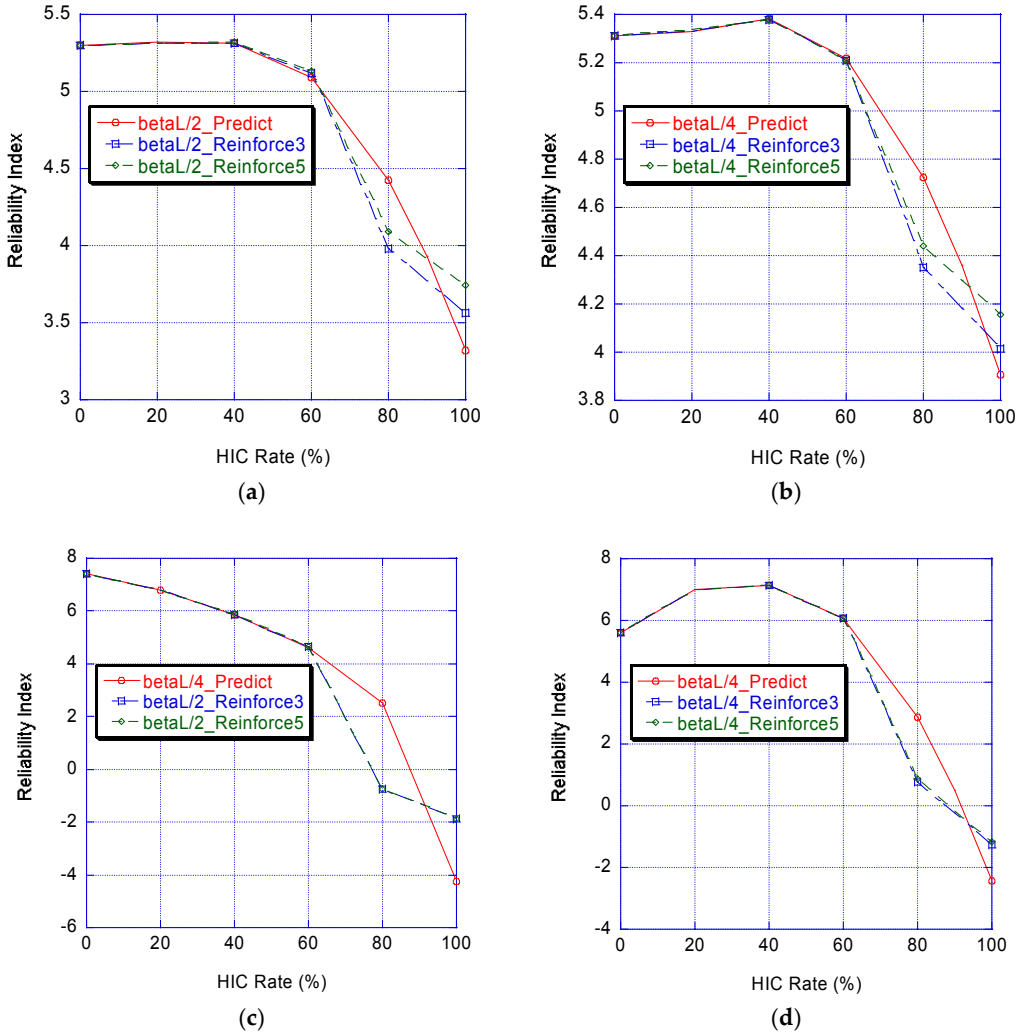


Figure 13. Inverse analysis results for the Bayesian belief network under 80% cracking in wire and reinforced for the cases when the reliability indices increased from: (i) 0.5 to 3.0; and (ii) 0.5 to 5.0. (**a**) Tensile stress at $L/2$. (**b**) Tensile stress at $L/4$. (**c**) Shear stress at $L/2$. (**d**) Shear stress at $L/4$.

It is notable that, compared with the tensile responses, the shear responses indicate higher safety, as the reliability indices increased from 128% and 80%, as increased from -4.25 to -1.86 and from -2.44 to -1.35 in reliability indices, under 100% cracking of the cable wires at $L/2$ and $L/4$, respectively. The tensile responses indicate considerably higher safety levels, as the reliability indices increased from 8.3% and 12.7%, as increased from 3322 to 3600 and from 3322 to 3744 in reliability indices, under 100% cracking of the cable wires at $L/2$, and approximately 5% increased safety at $L/4$. Therefore, it is acknowledged that the shear response is very sensitive to crack propagation in the main cable wires regardless of whether maintenance tasks are carried out.

In Table 3, the numbers of the columns in 25% and 50% reinforced girder represent the mean value of the simulated tensile stresses, shear stresses and cracking. Standard deviations are calculated from the distribution of MCMC results. The importance of the table lies on the comparison of the correlation among response values between the two 25% and 50% reinforced girder cases. Note that even if the responses of tensile stresses have decreased from 4.96 to 3.72 and 2.51, respectively, in terms of the reliability indices, the correlations between tensile and shear stresses are almost unchanged, as summarized in Table 3.

Table 3. Predicted simulation results between tensile and shear responses.

Predicted Variables	Base Variables	25% Reinforced Girder	Standard Deviation (25%)	Correlation (25%)	50% Reinforced Girder	Standard Deviation (50%)	Correlation (50%)
Tensile Stress	Tensile Stress	3.722	0.3722	1	2.48	0.248	1
Tensile Stress	Cracking in cable wires	3.722	0.3722	0.8138	2.48	0.248	0.8138
Tensile Stress	Shear Stress	3.722	0.3722	0.6945	2.48	0.248	0.6945
Cracking in cable wires	Tensile Stress	0.5	0.05	0.8138	0.5	0.05	0.8138
Cracking in cable wires	Cracking in cable wires	0.5	0.05	1	0.5	0.05	1
Cracking in cable wires	Shear Stress	0.5	0.05	0.8993	0.5	0.05	0.8993
Shear Stress	Tensile Stress	2.5052	0.2502	0.6945	2.5052	0.2502	0.6945
Shear Stress	Cracking in cable wires	2.5052	0.2502	0.8993	2.5052	0.2502	0.8993
Shear Stress	Shear Stress	2.5052	0.2502	1	2.5052	0.2502	1

4. Conclusions

A quantitative correlation model was developed and applied for analyzing correlation between hydrogen-induced corrosion cracking in the main cable wires of a cable suspension bridge with degraded stiffening girders, considering the effects of maintenance efforts in time and space. Bayesian inference was applied for predicting the correlation among wires in the main cables owing to HIC of the cable wires of a suspension bridge, by using the improved nonlinear hierarchical Bayesian models developed here, which is based on the Markov Chain Monte Carlo method.

The effects of maintenance interventions for alleviating cracking in the main cable wires due to HIC have been investigated using the developed inverse Bayesian prediction model. While reinforcing the main cable wires, in terms of reliability indices, from negative values to 3.0 and 5.0, the shear responses indicate considerably higher increase in safety than do tensile responses, as the reliability indices increased from 128% and 80% under 100% cracking of the cable wires at $L/2$ and $L/4$, respectively. Therefore, it is acknowledged that shear responses are very sensitive responses to the crack propagation in the main cable wires.

Consequently, the correlations between local corrosion and crack growth in high-strength steel in terms of crack propagation in the main cable wire of a suspension bridge with global responses of the structure are modeled for predicting future degradation, followed by inverse analysis for identifying the effects of maintenance interventions. The proposed inverse Bayesian inference model as the quantified correlation model not only provides highly improved convergence but also shows the possibility of future maintenance control and savings by offering infrastructure managers the opportunity of risk prognosis and mitigation.

Acknowledgments: This research was supported by Human resources Exchange program in Scientific technology through the National Research Foundation of Korea (NRF) funded by the Ministry of Science, ICT and future Planning (No. 2017H1D2A2000600).

Author Contributions: Taejun Cho, David Joaquin Delgado-Hernandez and Tae-Soo Kim conceived and designed the works; Taejun Cho, David Joaquin Delgado-Hernandez and Byung-Jik Son performed the numerical analysis; Kwan-Hyeong Lee and Byung-Jik Son analyzed the data; Taejun Cho, David Joaquin Delgado-Hernandez and Kwan-Hyeong Lee contributed reagents/materials/analysis tools; Taejun Cho and Tae-Soo Kim wrote the paper.

Conflicts of Interest: The authors declare no conflict of interest.

Appendix A

Table A1. Percentile, mean, standard deviation, and error of MCMC, simulation for Figure 11.

Stochastic Variables	Mean	Standard Deviation	Monte-Carlo Error	Lower Limit (2.5 Percent)	Median	Lower Limit (97.5 Percent)
mu[1,1]	24.52	700	19.03	3.221	5.511	7.847
mu[1,2]	16.57	421.6	11.47	3.377	5.109	6.871
mu[1,3]	8.608	143.1	3.902	3.331	4.714	6.091
mu[1,4]	0.6498	135.4	3.662	2.89	4.321	5.664
mu[1,5]	−7.308	413.8	11.23	2.087	3.922	5.618
mu[1,6]	−11.29	553.1	15.01	1.611	3.719	5.678
mu[1,7]	−15.27	692.3	18.79	1.105	3.517	5.775
mu[2,1]	24.31	689.1	18.76	3.233	5.576	7.939
mu[2,2]	16.54	415.2	11.31	3.479	5.243	7.02
mu[2,3]	8.765	141.4	3.862	3.517	4.911	6.296
mu[2,4]	0.9903	132.6	3.586	3.145	4.582	5.944
mu[2,5]	−6.784	406.5	11.03	2.393	4.252	5.971
mu[2,6]	−10.67	543.4	14.76	1.927	4.089	6.067
mu[2,7]	−14.56	680.3	18.48	1.439	3.924	6.207
mu[3,1]	22.41	691.5	18.8	1.353	3.616	6.012
mu[3,2]	13.9	416.7	11.34	0.8279	2.561	4.442
mu[3,3]	5.393	142	3.872	0.1083	1.504	3.071
mu[3,4]	−3.116	132.9	3.595	−0.9538	0.4491	2.024
mu[3,5]	−11.63	407.6	11.06	−2.336	−0.6043	1.293
mu[3,6]	−15.88	545	14.79	−3.107	−1.129	1.006
mu[3,7]	−20.13	682.4	18.53	−3.914	−1.654	0.744
mu[4,1]	27.69	704.9	19.18	5.92	8.566	10.93
mu[4,2]	18.19	424.7	11.57	4.733	6.661	8.414
mu[4,3]	8.69	144.5	3.947	3.351	4.754	6.109
mu[4,4]	−0.8083	135.8	3.671	1.499	2.852	4.244
mu[4,5]	−10.31	415.9	11.29	−0.8075	0.9476	2.832
mu[4,6]	−15.06	556	15.1	−2.063	−0.00627	2.211
mu[4,7]	−19.8	696.2	18.91	−3.336	−0.9572	1.638

References

1. Hopwood, T.; Havens, J.H. Corrosion of Cable Suspension Bridges. Available online: http://uknowledge.uky.edu/cgi/viewcontent.cgi?article=1666&context=ktc_researchreports (accessed on 30 May 2017).
2. Roffey, P. The fracture mechanisms of main cable wires from the forth road suspension. *Eng. Fail. Anal.* **2013**, *31*, 430–441. [CrossRef]
3. Cho, T.; Kim, T.S.; Lee, D.H.; Han, S.H.; Choi, J.H. Reliability analysis of a suspension bridge affected by hydrogen induced cracking based upon response surface method. *ISIJ Int.* **2009**, *49*, 1414–1423. [CrossRef]
4. Cho, T.; Kim, T.S. A prediction model for hydrogen induced cracking in a prestressed wire with a fracture analysis. *ISIJ Int.* **2008**, *48*, 496–505. [CrossRef]
5. Laureys, A.; Depover, T.; Petrov, R.; Verbeken, K. Influence of sample geometry and microstructure on the hydrogen induced cracking characteristics under uniaxial load. *Mater. Sci. Eng. A* **2017**, *690*, 88–95. [CrossRef]
6. Masoumi, M.; Silva, C.C.; de Abreu, H.F.G. Effect of crystallographic orientations on the hydrogen-induced cracking resistance improvement of API 5L X70 pipeline steel under various thermomechanical processing. *Corros. Sci.* **2016**, *111*, 121–131. [CrossRef]
7. Dunne, D.P.; Hejazi, D.; Saleh, A.A.; Haq, A.J.; Calka, A.; Pereloma, E.V. Investigation of the effect of electrolytic hydrogen charging of X70 steel: I. The effect of microstructure on hydrogen-induced cold cracking and blistering. *Int. J. Hydrog. Energy* **2016**, *41*, 12411–12423. [CrossRef]
8. Laureys, A.; Depover, T.; Petrov, R.; Verbeken, K. Characterization of hydrogen induced cracking in TRIP-assisted steels. *Int. J. Hydrog. Energy* **2015**, *40*, 16901–16912. [CrossRef]

9. Shi, X.; Yan, W.; Wang, W.; Zhao, L.; Shan, Y.; Yang, K. Effect of microstructure on hydrogen induced cracking behavior of a high deformability pipeline steel. *J. Iron Steel Res. Int.* **2015**, *22*, 937–942. [CrossRef]
10. Koch, G.H. Fatigue and fracture. *ASM Handb.* **1996**, *19*, 483–506.
11. Tsai, W.T.; Chou, S.L. Environmentally assisted cracking behavior of duplex stainless steel in concentrated sodium chloride solution. *Corros. Sci.* **2000**, *42*, 1741–1762. [CrossRef]
12. Mohtadi-Bonab, M.A.; Szpunar, J.A.; Razavi-Tousi, S.S. A comparative study of hydrogen induced cracking behavior in API 5L X60 and X70 pipeline steels. *Eng. Fail. Anal.* **2013**, *33*, 163–175. [CrossRef]
13. Gjerding-Smith, K.; Johnsen, R.; Lange, H.I.; Leinum, B.H.; Gundersen, G.; Isaksen, B.; Nærum, G. Wire fractures in locked coil cables. *Bridge Struct.* **2006**, *2*, 63–77. [CrossRef]
14. Cho, T.; Kim, T.S. Probabilistic risk assessment for the construction phases of a bridge construction based on finite element analysis. *Finite Elem. Anal. Des.* **2008**, *44*, 383–400. [CrossRef]
15. LaFrance-Linden, D.; Watson, S.; Haines, M. Threat Assessment of Hazardous Materials Transportation in Aircraft Cargo Compartments. *Transp. Res. Rec.* **2001**, *1763*, 130–137. [CrossRef]
16. Sundararajan, C. *Probabilistic Structural Mechanics Handbook*; Chapman & Hall: London, UK, 1994.
17. Nowak, A.S.; Cho, T. Prediction of the combination of failure modes for an arch bridge system. *J. Constr. Steel Res.* **2007**, *63*, 1561–1569. [CrossRef]
18. Cho, T.; Song, M.-K.; Lee, D.H. Reliability analysis for the uncertainties in vehicle and high-speed railway bridge system based on an improved response surface method for nonlinear limit states. *Nonlinear Dyn.* **2010**, *59*, 1. [CrossRef]
19. Bayes, T.; Price, R.; Canton, J. An essay towards solving a problem in the doctrine of chances. *Philos. Trans.* **1763**, *53*, 370–418. [CrossRef]
20. Mayrbaurl, R.M.; Camo, S. Cracking and Fracture of Suspension Bridge Wire. *J. Bridge Eng.* **2001**, *6*, 645–650. [CrossRef]
21. Toribio, J. Hydrogen embrittlement of prestressing steels: the concept of effective stress in design. *Mater. Des.* **1997**, *18*, 81–85. [CrossRef]
22. Forman, R.G.; Shivakuma, V. Growth Behavior of Surface Cracks in the Circumferential Plane of Solid and Hollow Cylinders. In *Fracture Mechanics: Seventeenth Volume*; ASTM International: West Conshohocken, PA, USA, 1986; p. 59.
23. Forman, R.G.; Shivakumar, V.; Newman, J.C., Jr. *Fatigue Crack Growth Computer Program*; NASA/FLAGRO: Houston, TX, USA, 1994.
24. Bucher, C.G.; Bourgund, U. *Efficient Use of Response Surface Methods*; Report No. 9-87; University of Innsbruck: Innsbruck, Austria, 1987.
25. Sagues, A.A.; Wang, H. *Corrosion of Post Tensioning of Strands*; Florida Department of Transportation: Tallahassee, FL, USA, 2005; p. 255.



© 2017 by the authors. Licensee MDPI, Basel, Switzerland. This article is an open access article distributed under the terms and conditions of the Creative Commons Attribution (CC BY) license (http://creativecommons.org/licenses/by/4.0/).